



Cartilage-inspired self-assembly glycopeptide hydrogels for cartilage regeneration via ROS scavenging

Zhijian Zhao^{a,b,1}, Xiaowei Xia^{a,b,1}, Junlin Liu^{a,b,1}, Mingzhuang Hou^{a,b}, Yang Liu^{a,b}, Zhangzhe Zhou^{a,b}, Yong Xu^{a,b}, Fan He^{a,b}, Huilin Yang^{a,b}, Yijian Zhang^{a,b,*}, Changshun Ruan^{c,d,**}, Xuesong Zhu^{a,b,***}

^a Department of Orthopaedics, The First Affiliated Hospital of Soochow University, Soochow University, Suzhou, 215006, China

^b Orthopaedic Institute, Medical College, Soochow University, Suzhou, 215007, China

^c Center for Human Tissue and Organs Degeneration, Institute of Biomedicine and Biotechnology, Shenzhen Institute of Advanced Technology, Chinese Academy of Sciences, Shenzhen, 518055, China

^d University of Chinese Academy of Sciences, Beijing, 100049, China

ARTICLE INFO

Keywords:

Cartilage repair
Self-assembly glycopeptide hydrogels
Fucoidan
ROS scavenging

ABSTRACT

Cartilage injury represents a frequent dilemma in clinical practice owing to its inherently limited self-renewal capacity. Biomimetic strategy-based engineered biomaterial, capable of coordinated regulation for cellular and microenvironmental crosstalk, provides an adequate avenue to boost cartilage regeneration. The level of oxidative stress in microenvironments is verified to be vital for tissue regeneration, yet it is often overlooked in engineered biomaterials for cartilage regeneration. Herein, inspired by natural cartilage architecture, a fibril-network glycopeptide hydrogel (Nap-FFGRGD@FU), composed of marine-derived polysaccharide fucoidan (FU) and naphthalenophenylalanine-phenylalanine-glycine-arginine-glycine-aspartic peptide (Nap-FFGRGD), was presented through a simple supramolecular self-assembly approach. The Nap-FFGRGD@FU hydrogels exhibit a native cartilage-like architecture, characterized by interwoven collagen fibers and attached proteoglycans. Beyond structural simulation, fucoidan-exerted robust biological effects and Arg-Gly-Asp (RGD) sequence-provided cell attachment sites realized functional reinforcement, synergistically promoted extracellular matrix (ECM) production and reactive oxygen species (ROS) elimination, thus contributing to chondrocytes-ECM harmony. *In vitro* co-culture with glycopeptide hydrogels not only facilitated cartilage ECM anabolic metabolism but also scavenged ROS accumulation in chondrocytes. Mechanistically, the chondro-protective effects induced by glycopeptide hydrogels rely on the activation of endogenous antioxidant pathways associated with nuclear factor erythroid 2-related factor 2 (NRF2). *In vivo* implantation of glycopeptide hydrogels successfully improved the *de novo* cartilage generation by 1.65-fold, concomitant with coordinately restructured subchondral bone structure. Collectively, our ingeniously crafted bionic glycopeptide hydrogels simultaneously rewired chondrocytes' function by augmenting anabolic metabolism and rebuilt ECM microenvironment via preserving redox equilibrium, holding great potential for cartilage tissue engineering.

1. Introduction

Damage to the thin cartilage that lines the ends of bones is referred to

as articular cartilage injury; it is a result of a knee collision or trauma or occurs in conjunction with other knee joint injuries [1]. The overall prevalence of cartilage injuries in athletes is estimated to be as high as

Peer review under responsibility of KeAi Communications Co., Ltd.

* Corresponding author. Department of Orthopaedics, The First Affiliated Hospital of Soochow University, No. 899 Pinghai Road, Suzhou, 215006, Jiangsu, China.

** Corresponding author. Center for Human Tissue and Organs Degeneration, Institute of Biomedicine and Biotechnology, Shenzhen Institute of Advanced Technology, Chinese Academy of Sciences, Shenzhen, 518055, China.

*** Corresponding author. Department of Orthopaedics, The First Affiliated Hospital of Soochow University, No. 899 Pinghai Road, Suzhou, 215006, Jiangsu, China.

E-mail addresses: zhangyijian@suda.edu.cn (Y. Zhang), cs.ruan@siat.ac.cn (C. Ruan), zhuxs@suda.edu.cn (X. Zhu).

¹ ZZ, XX, and JL contributed equally to this work.

<https://doi.org/10.1016/j.bioactmat.2023.10.013>

Received 21 June 2023; Received in revised form 10 October 2023; Accepted 10 October 2023

2452-199X/© 2023 The Authors. Publishing services by Elsevier B.V. on behalf of KeAi Communications Co. Ltd. This is an open access article under the CC BY-NC-ND license (<http://creativecommons.org/licenses/by-nc-nd/4.0/>).

36 % [2]. Most patients are limited in their activities, referred to as “locking knee”, because of the presence of loose bodies floating within the joints, rather than recurrent pain or audible clunks [3]. Current treatment approaches for cartilage injuries include conservative management, i.e., oral or topical analgesics, or transplantation-based surgical strategies [4]. Nonetheless, considering the limited capacity of cartilage self-repair, the existing therapies have proved disappointing. Bio-inspired materials are being developed to create bio-adaptive matrices that facilitate tissue regeneration. The natural architecture of cartilage’s extracellular matrix (ECM) is composed of a collagenous network and proteoglycans, which synergistically define its mechanical properties with exquisite elegance [5]. Accordingly, collagen-derived proteins such as gelatin and gelatin methacryloyl (GelMA) hydrogels are widely employed as ideal substrates due to their excellent biocompatibility and biodegradability for cartilage tissue engineering (CTE) [6]. Recently, peptide-based supramolecular hydrogels have exhibited tremendous potential in the fields of drug delivery and tissue regeneration [7]. Through non-covalent interactions, minute molecules can self-organize and generate functional entities with the remarkable properties of shear-thinning and immediate recovery, rendering them the optimal carriers for drug delivery via an injectable approach [8]. Significantly, the rational design of amino acid sequences and peptide secondary structural domains can yield bespoke physicochemical performance under diverse circumstances [9]. Therefore, peptide-based hydrogels that mimic the structure of cartilage ECM have the potential to emerge as a novel contender for cartilage repair.

When cartilage is injured, an inflammatory response triggers an endogenous repair process in the affected area. However, this process is accompanied by excessive production of reactive oxygen species (ROS) or MMPs [10], the aforementioned factors are accountable for disrupting the extracellular matrix of cartilage, consequently exacerbating the progression of osteoarthritis (OA) [11]. It is widely acknowledged that the accumulation of ROS not only serves as a detrimental factor for cartilage degeneration, but also impedes the lineage commitment of mesenchymal stem cells (MSCs) towards chondrocytes [12]. Despite the emphasis on enhancing cellular recruitment or promoting chondrogenic differentiation in cartilage repair, the crucial role of a harsh oxidative stress microenvironment is often overlooked. Refocusing on the removal of endogenous ROS to create a more conducive environment for annulus fibrosus (AF) regeneration holds great potential in treating intervertebral disc degeneration (IVDD) [13]. Similarly, the scaffolds infused with functional metal-organic frameworks (MOFs), such as zinc-cobalt (Zn/Co) [14], exhibit robust antioxidant properties that enhance the regeneration of cartilage and subchondral bone in refractory osteochondral defects. The marine-derived polysaccharide fucoidan, extracted from brown seaweeds, exhibits remarkable efficacy in the treatment of wound healing [15] and inflammatory diseases [16], owing to its inherent anti-inflammatory and immune-modulating properties. Since the presence of negatively charged ester-linked sulphate groups, sulfated fucoidan exhibits remarkable antioxidant activity in Fenton systems and is thus regarded as an efficient scavenger of ROS [17]. Moreover, long-term use of glucosamine sulphate, a natural compound found in cartilage, can reduce pain symptoms and act as a disease modifier agent for cartilage disorders [18,19]. With its unique sulphate structure resembling the natural components of chondroitin sulphate (CS) within ECM, fucoidan is recognized as a promising candidate for cartilage rejuvenation. The composite hydrogels enhanced by fucoidan mimics a natural ECM tailored to the cellular microenvironment [20] and promotes chondrogenic differentiation of MSCs [21]. Thus, the incorporation of fucoidan presents a significant potential for strengthened dual-effects on ROS scavenging and ECM regeneration for cartilage repair.

In this study, inspired that proteoglycan and collagen were randomly interleaved within natural cartilage, the glycopeptide hydrogels, made up of self-assembling peptide (Nap-FFGRGD) [22] for collagen fibrils substitute and polysaccharide (fucoidan) as alternative staggered

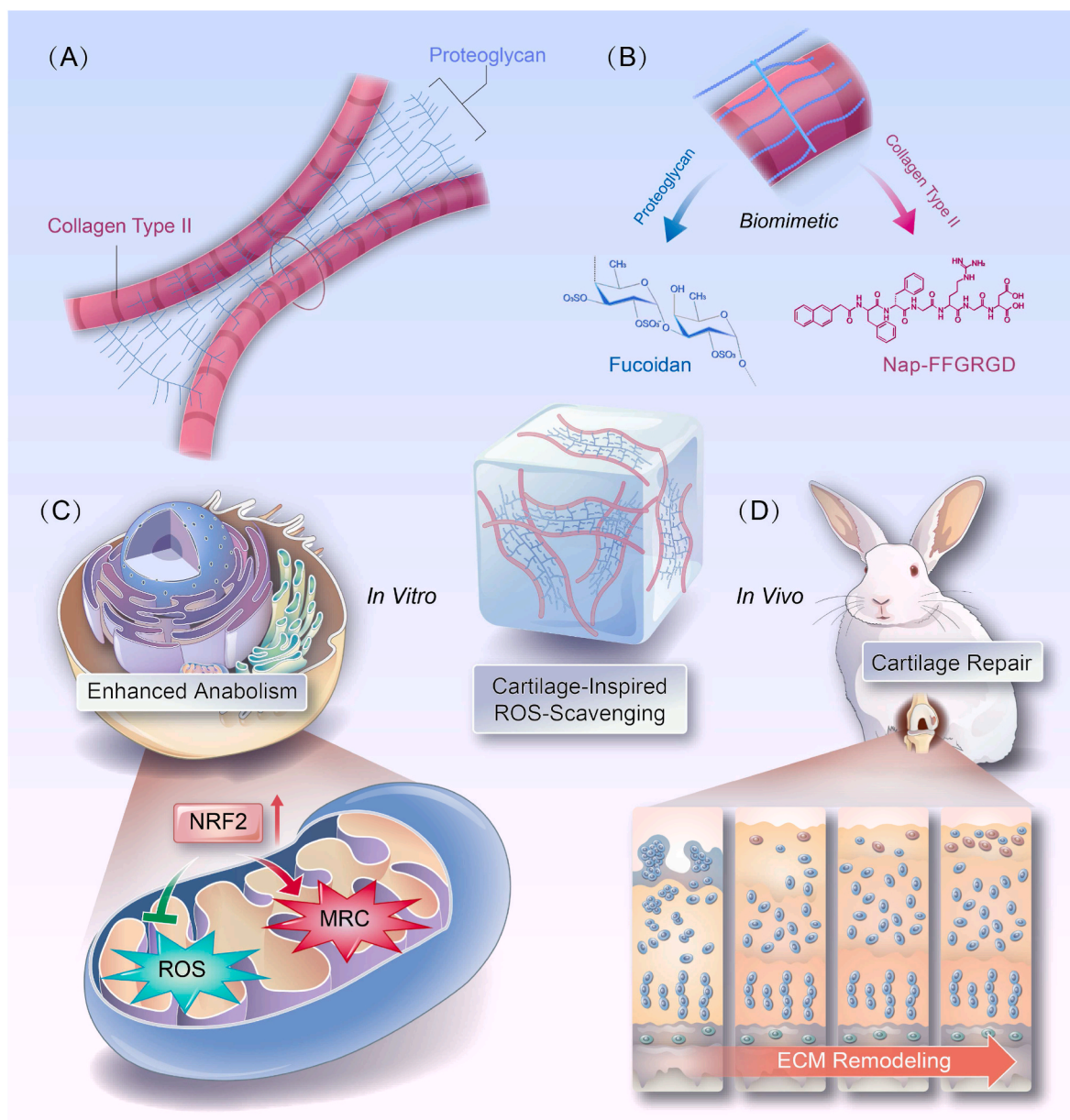
arranged proteoglycans, were skillfully designed using a supramolecular self-assembly reaction (Scheme 1). The self-assembled peptides, enriched with RGD residues, should create a conducive microenvironment for *in situ* stem cells, thereby initiating an augmented regenerative response toward injury. Furthermore, the bioactive fucoidan sustainably released from hydrogels can provide dual biological cues by promoting ECM secretion and scavenging overproduced ROS simultaneously, thus exhibiting an exquisite balance between tissue regeneration and oxidative stress management. Thus, our biomimetic glycopeptide hydrogels will exhibit enhanced crosstalk of chondrocytes and cartilage ECM, demonstrating great potential for rational cartilage regeneration.

2. Results and discussion

2.1. Preparation and characterization of self-assembly glycopeptide hydrogels

To elucidate the microstructure of cartilage ECM, a porcine femoral head was meticulously isolated and subjected to meticulous scanning electron microscopy (SEM) analysis. Natural cartilage ECM is composed of a heterogeneous and anisotropic alignment of collagen fibers, creating an intricate structure (Fig. 1A). Subsequently, as observed through SEM and transmission electron microscopy (TEM) analyses, the self-assembling glycopeptide hydrogels exhibited micro/nanostructures strikingly similar to those found in natural cartilage (Fig. 1B). Meanwhile, after modification with fucoidan, the ultrastructural morphology by SEM had a 28.4 % lower pore size (Fig. S1A). TEM images revealed a 3D network made up of entangled nanofibers with a diameter ranging between 10 and 15 nm (Fig. S1B). Elemental mapping analysis indicated the presence of sulfur in Nap-FFGRGD@FU, thus confirming the successful anchoring of fucoidan (Fig. 1C). The formation of hydrogels from the solution was unveiled by means of a simple thermal cycling process (Fig. 1D). Based on FTIR analysis, the characteristic peaks at 1544 cm^{-1} and 1639 cm^{-1} represented the backbone of the self-assembling peptide [23,24]. Moreover, the peaks of sulfation were represented by $\text{S}=\text{O}$ at 1034 cm^{-1} and $\text{C}-\text{O}-\text{S}$ at 820 cm^{-1} , accompanied by the fucoidan-specific $\text{S}-\text{O}$ peaks [25] at 1250 cm^{-1} (Fig. S2). Rheological sweep revealed the kinetics of supramolecular hydrogelation, where the storage modulus (G') was larger than the loss modulus (G''), indicating a successful formation of a solid-like hydrogel (Fig. S3). Furthermore, the self-assembling glycopeptide hydrogels exhibit a remarkable ability to form and possess an excellent injectable property even in moist environments (Fig. S4). According to the compressive test, a remarkable enhancement in the mechanical modulus upon incorporating fucoidan was revealed, effectively compensating for the limited mechanical properties of self-assembly glycopeptide hydrogels (Fig. S5). Overall, fucoidan imparts polysaccharide-like properties to self-assembly hydrogel, tactfully forming a glycopeptide complex to mimic natural cartilage ECM.

Fucoidan release and hydrogel degradation were comprehensively determined through *in vitro* and *in vivo* models. The hydrogel integrity remained intact when exposed to PBS solution for up to 3 weeks; however, more than half of the hydrogel degraded within 7 days and only approximately 10 % remained after incubation with collagenases for 3 weeks (Fig. 1E–F). A chronological release pattern was observed for fucoidan encapsulated within hydrogels using a toluidine blue O (TBO)-based colorimetric method as previously reported [26] (Fig. S6). The physically mixed fucoidan in hydrogels showed a rapid release rate of 33 % within the first stage, occurring within 24 h (Fig. 1G). In the subsequent three weeks, the resident two thirds of crosslinked fucoidan through hydrogen bonds were gradually released as the hydrogels underwent degradation (Fig. 1H). Importantly, concentration monitoring assays indicated that though fucoidan concentration was decreased gradually accompanied with culture medium update, the dynamic range could perfectly match the therapeutic windows of fucoidan (Fig. 1I) [27–29]. The *in vivo* retention experiments further demonstrated that



Scheme 1. Schematic illustration depicting the preparation and application of a self-assembly glycopeptide hydrogels to facilitate cartilage regeneration. Inspired by the intricate architecture of natural cartilage (A), a cleverly crafted glycopeptide hydrogel composed of self-assembling peptide (Nap-FFGRGD) and polysaccharide (fucoidan), mimicking collagen and proteoglycans, was ingeniously designed (B). The bionic glycopeptide hydrogels enhanced chondrocyte function by boosting anabolic metabolism (C) and reconstructed the ECM microenvironment through maintaining redox equilibrium (D), thus serving as a viable alternative for cartilage regeneration.

the hydrogels exhibited a responsive behavior towards highly activated enzymes present in the joint cavity during the initial week, gradually undergoing slow degradation within three weeks, both in sham and posttraumatic OA mice (Fig. 1J–K). In summary, glycopeptide hydrogels exhibited the remarkable ability to orchestrate a dual-phase release of fucoidan, thereby eliciting both an “immediate response” and “sustained maintenance” for optimal cartilage regeneration.

2.2. Glycopeptide hydrogels recoupled cartilage ECM metabolism by releasing fucoidan

Rabbit-derived chondrocytes were co-cultured with low- or high-concentration fucoidan hydrogels to assess the impact of glycopeptide hydrogels on the equilibrium of cartilage ECM using a Transwell co-culture system (Fig. S7A). Cell viability experiments revealed

favorable biocompatibility of these glycopeptide hydrogels (Figs. S7B–C). Meanwhile, chondrocytes proliferation (Fig. S7D) or morphology (Fig. S7E) was barely affected by co-culture with hydrogels. Alcian blue staining revealed a higher glycosaminoglycan (GAG) level in the Nap-FFGRGD@FU_H group compared to the untreated group (Fig. 2A). Similarly, collagen type II (COLII) expression in chondrocytes was significantly improved when cultured in the high-concentration fucoidan hydrogels (Fig. 2B–C). To evaluate the beneficial effects of conjugated RGD sequence on cellular adhesion, chondrocytes were seeded onto Nap-FFG (RGD⁻) or Nap-FFGRGD (RGD⁺), respectively. The RGD-modified self-assembly hydrogels, as anticipated, offered adhesive sites to facilitate cellular proliferation and spreading (Fig. S8). The Transwell migration and scratch assay further suggested that fucoidan exhibited enhanced efficacy in promoting cell recruitment (Fig. 2D–F), thereby establishing a solid foundation for subsequent “cell

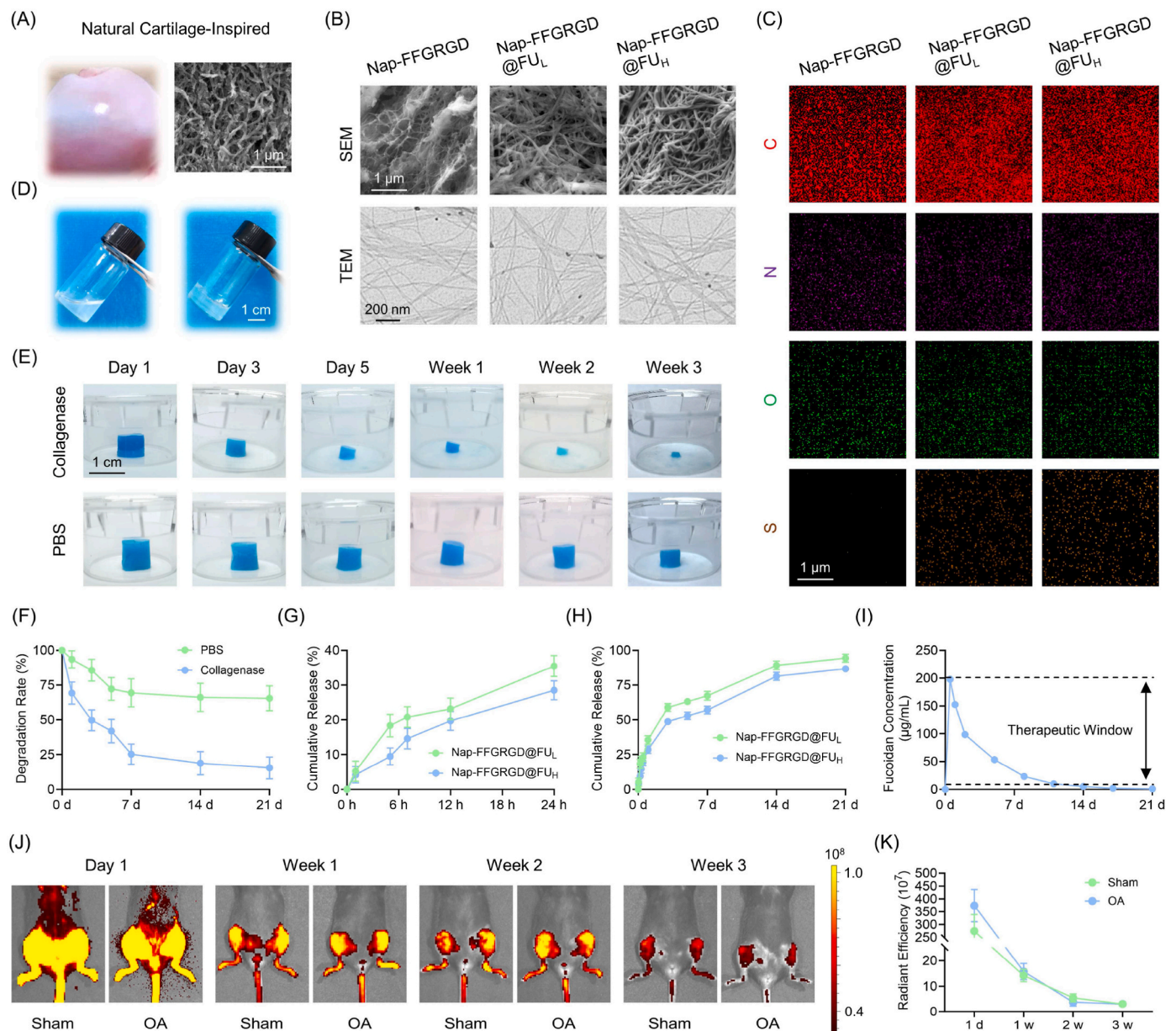


Fig. 1. Preparation and characterization of self-assembly glycopeptide hydrogels. (A) The gross and SEM images of natural cartilage derived from porcine femur head. (B) Representative images of the ultrastructure of glycopeptide hydrogels by SEM and TEM. (C) The distribution of the major elements within glycopeptide hydrogels. (D) Optical images of the gel formation with a heating-cooling process-induced supermolecular self-assembly. (E–F) The degradation rate of hydrogels in PBS or collagenase-mimicking injury microenvironment ($n = 3$). (G–H) The release profile of fucoidan during the initial 24 h (stage I) and the subsequent three weeks (stage II) ($n = 3$). (I) The concentration of fucoidan in the culture medium was ascertained within three weeks. (J–K) *In vivo* distribution and retention of injected hydrogels in sham or OA mice within three weeks ($n = 5$). Data are presented as mean \pm SD (* $P < 0.05$ or ** $P < 0.01$ between the indicated groups).

homing” during *in situ* implantation at the defect site [30]. Additionally, the expression level of collagen type X (COLX) was effectively suppressed in the chondrocytes treated with a high-concentration fucoidan hydrogels (Fig. 2G). Co-culturing with glycopeptide biomimetic hydrogels led to a significant increase in cartilage ECM synthesis markers at both the transcriptional and translational levels (Fig. 2H&J&S9A), accompanied by a reduction in ECM degradation enzymes (Fig. 2I&K&S9B), suggesting that fucoidan facilitates a reorganized metabolic homeostasis of the ECM. Among the many natural polymers, fucoidan generated from seaweed is of abundant reserves due to the rich marine resources, providing promising future applications [31]. The composition and structure of fucoidan are diverse owing to the discrepancy between seaweed species, and geographic or anatomical

regions. Fucoidans from the seaweed *Fucus vesiculosus* L., *Macrocystis pyrifera* L., or *Undaria pinnatifida* exert similar but not identical protective effects on OA fibroblast-like synoviocytes by regulating growth factor-beta (TGF- β)/SMAD signaling pathway [32]. The treatment benefits of fucoidan on collagen-induced arthritis depend on different molecular weights; for instance, low molecular weight fucoidan alleviates arthritis by suppressing T helper 1 (Th1)-mediated immune reactions [33]. To facilitate the regeneration of cartilage, we utilized fucoidan extracted from *Fucus vesiculosus* L., a source renowned for its ability to impede the onset of osteoarthritis [29]. Although some studies have suggested that fucoidan treatment may promote the differentiation of MSCs into chondrocytes [22,34], the precise role of fucoidan-induced cartilage protection in the reconstruction of defects and the underlying

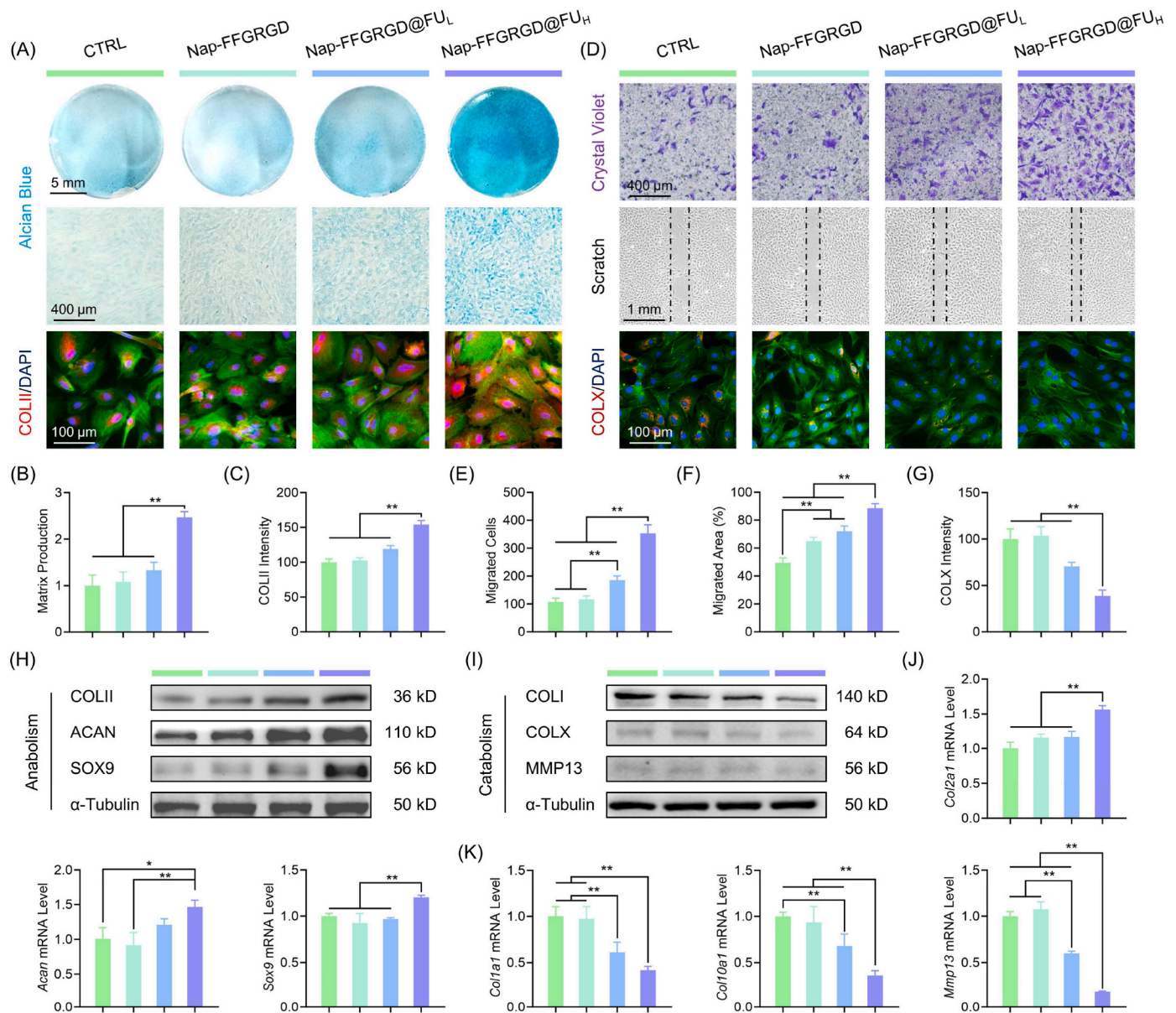


Fig. 2. Glycopeptide self-assembling hydrogels recoupled cartilage ECM metabolism *in vitro*. (A) Representative images of anabolic markers of chondrocytes stained by Alcian blue and COLII. (B–C) Quantitative assessment of matrix production level and intensity of COLII immunofluorescence ($n = 3$). (D) Representative images of cell migration determined by crystal violet and scratch assays, alongside the catabolic markers of chondrocytes stained by COLX. (E–G) Quantitative evaluation of the number of migrating cells, area covered by migration, and intensity of COLX immunofluorescence ($n = 3$). (H–I) Protein levels of COLII, ACAN, SOX9, COLI, COLX, and MMP13 were measured using western blot. (J–K) Gene expression of *Col2a1*, *Acan*, *Sox9*, *Col1a1*, *Col10a1*, and *Mmp13* was determined using RT-PCR assay ($n = 4$). Data are presented as mean \pm SD (* $P < 0.05$ or ** $P < 0.01$ between the indicated groups).

mechanisms involved remain elusive [35]. Therefore, further investigations into the regulatory effects of fucoidan on MSC fate should be pursued in future studies.

2.3. Glycopeptide hydrogels augmented the antioxidant properties and mitochondrial functions

Considering the robust production of ECM induced by fucoidan, we delved into the underlying mechanisms through which it exerts its effects. Based on this premise, we extracted the differentially expressed genes (DEGs) associated with cartilage degeneration from the Gene Expression Omnibus (GEO) database (GSE169077) to unveil potential molecular cascades underlying ECM degradation. The pooled findings revealed that the progression of ECM loss coincided with the modulation of chemokines belonging to the C–C motif superfamily, such as

chemokine ligand 4 (CCL4) and CCL20 (Fig. 3A&S10A) [36]. Further enrichment analysis implied the involvement of oxygen metabolism and oxidative stress in the cartilage degeneration (Fig. 3B–C&S10B–C). Elaborating on this, in degenerated cartilage samples, the expression levels of superoxide dismutase 1 (SOD1), SOD2, and SOD3 were significantly diminished when compared to those observed in normal patients (Fig. S10D). Accordingly, intricate redox balance pathways involving the generation of ROS and the presence of antioxidant elements were subsequently meticulously elucidated. Dichloro-dihydro-fluorescein diacetate (DCFH-DA) assay revealed that intracellular ROS were down-regulated in high-concentration fucoidan hydrogels (Fig. 3D). Furthermore, at the subcellular level, treatment with glycopeptide hydrogels effectively suppressed the generation of ROS in mitochondria. The activity of NRF2, an important regulator of antioxidant response was improved in the Nap-FFGRGD@FU_H group

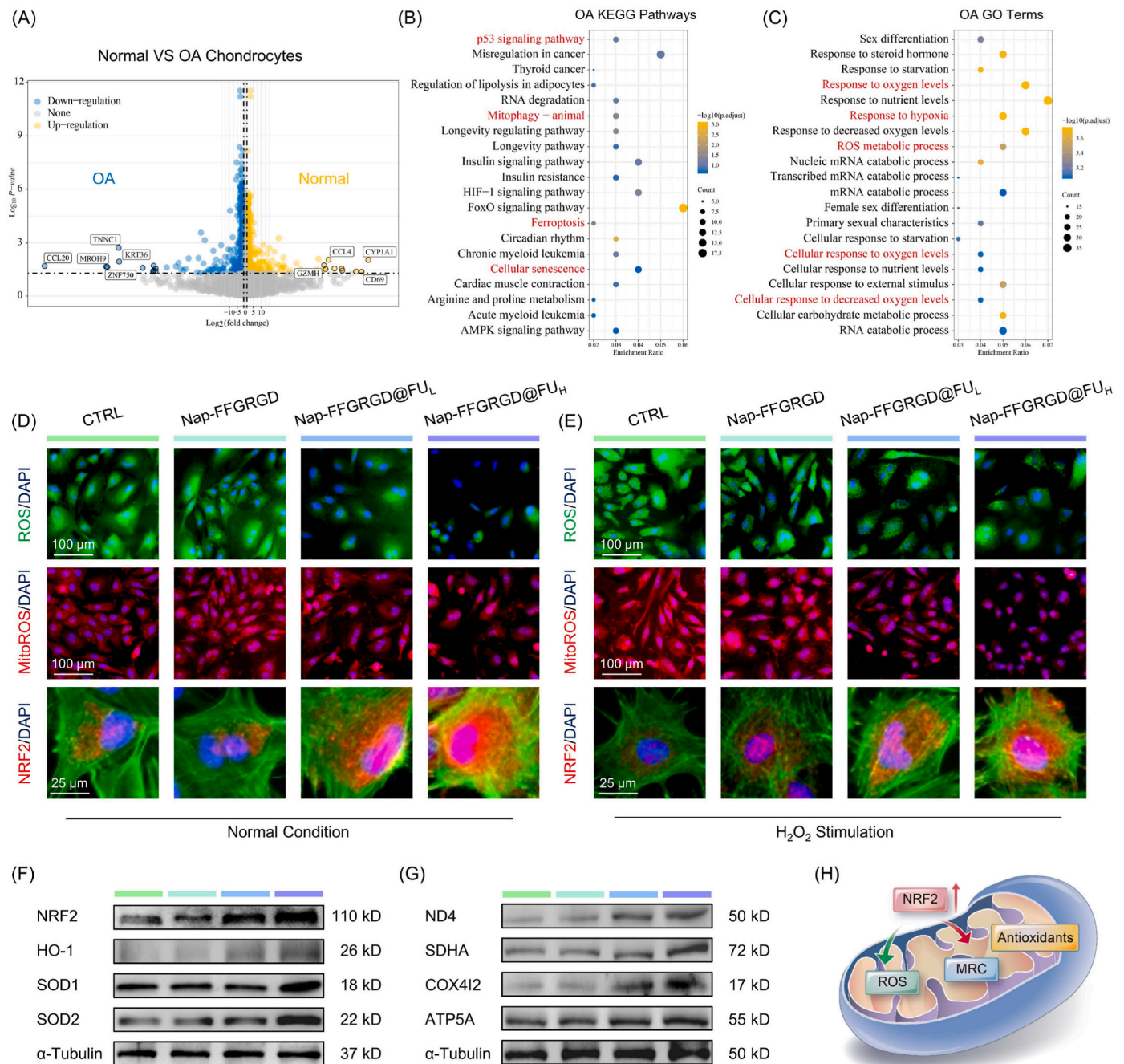


Fig. 3. Glycopeptide hydrogels attenuated ROS levels and advocated mitochondrial functions. (A) The volcano plot for differentially genes (DEGs) expression as OA progress. (B–C) Kyoto Encyclopedia of Genes and Genomes (KEGG) pathway analysis and Gene Ontology (GO) enrichment function analysis. (D–E) Representative images of chondrocytes stained by intracellular or mitochondrial ROS staining, and NRF2 immunofluorescence in normal or H₂O₂-stimulated oxidative stress environment. (F–G) Protein levels of antioxidant elements or MRC components were measured using western blot. (H) The glycopeptide hydrogels exhibit enhanced antioxidant properties and promoted mitochondrial respiration. Data are presented as mean \pm SD (**P* < 0.05 or ***P* < 0.01 between the indicated groups).

than in the untreated group (Fig. S11A). The efficacy of ROS elimination and NRF2 reinforcement was significantly demonstrated under the conditions of oxidative stress induced by H₂O₂ stimulation, highlighting the robust redox modulation exerted by fucoidan (Fig. 3E&S11B). RT-PCR and western blot experiments confirmed the motivation of glycopeptide hydrogels on intracellular antioxidant elements including heme oxygenase 1 (HO-1), SOD1, and SOD2 (Fig. 3F&S11C). As evidenced by the transcript and protein assay (Fig. 3G&S12), treatment with Nap-FFGRGD@FU_H resulted in improved mitochondrial respiratory chain (MRC) complex function in chondrocytes (Fig. 3H). The remarkable antioxidant properties of fucoidan are harnessed in a

nanofibrous scaffold, ingeniously designed to combat the inflammatory and oxidative microenvironment in IVDD [37]. Since mitochondria act as a primary source of free radicals, the maintenance of mitochondrial functions, particularly for MRC is indispensable. Mitochondrial dysregulation may cause cartilage degeneration by oxidative injury, defective chondrocyte biosynthesis, or matrix catabolism [38]. Our recent investigation has demonstrated that the targeting of sirtuins can effectively safeguard chondrocytes from OA-induced damage by reinvigorating dysfunctional mitochondria, thus emphasizing the crucial role of mitochondrial charging capacity in cartilage regeneration [39,40]. Nonetheless, the purified fucoidan from *Sargassum polycystum* induces

apoptosis through mitochondria-mediated DNA damage in tumorigenesis [41]. Therefore, further elucidation is required to understand how fucoidan modulates mitochondrial dynamics in chondrogenesis.

2.4. Glycopeptide hydrogels-induced cartilage protection was contingent upon NRF2 pathway

To unravel the crucial role of NRF2 in enhancing cellular antioxidant potency and promoting cartilage ECM synthesis, chondrocytes were pre-treated with ML385, a specific inhibitor of NRF2, prior to co-culturing with glycopeptide hydrogels. Immunofluorescence staining revealed that treatment with ML385 downregulated NRF2 expression compared with Nap-FFGRGD@FU_H-treated chondrocytes (Fig. 4A–B). NRF2 mRNA and protein levels were found to be downregulated following ML385 treatment (Fig. 4C–D). Moreover, the expression levels of antioxidant components downstream of the NRF2 pathway were suppressed

(Fig. 4E&S13A). The treatment of ML385 resulted in a simultaneous down-regulation of GAG and COLII expression, while up-regulating the level of COLX in chondrocytes (Fig. 4F–G). Disruption of anabolism and catabolism by NRF2 knockdown was verified at the transcript or translational levels (Fig. 4H&S13B–C). By binding to the specific antioxidant response element (ARE) in the nucleus, NRF2 orchestrates a vast array of proteins involved in antioxidant and anti-inflammatory defenses, as well as safeguarding our mitochondria. Global deletion of *Nrf2* *in vivo* aggravates oxidative stress injury and cartilage degradation in rheumatoid arthritis (RA) [42], and promotes cartilage ECM loss through secretion of proteinases and proinflammatory cytokines in OA [43]. Our previous study revealed that anti-arthritis effects induced by kartogenin (KGN), a chondrogenic molecule in OA depend on NRF2 upregulation at its post-transcript level [44]. NRF2/HO-1-related antioxidant signaling systems play a role in the fucoidan-mediated prevention of kidney diseases [45]. Arguably, this study unveiled the protective potential of the

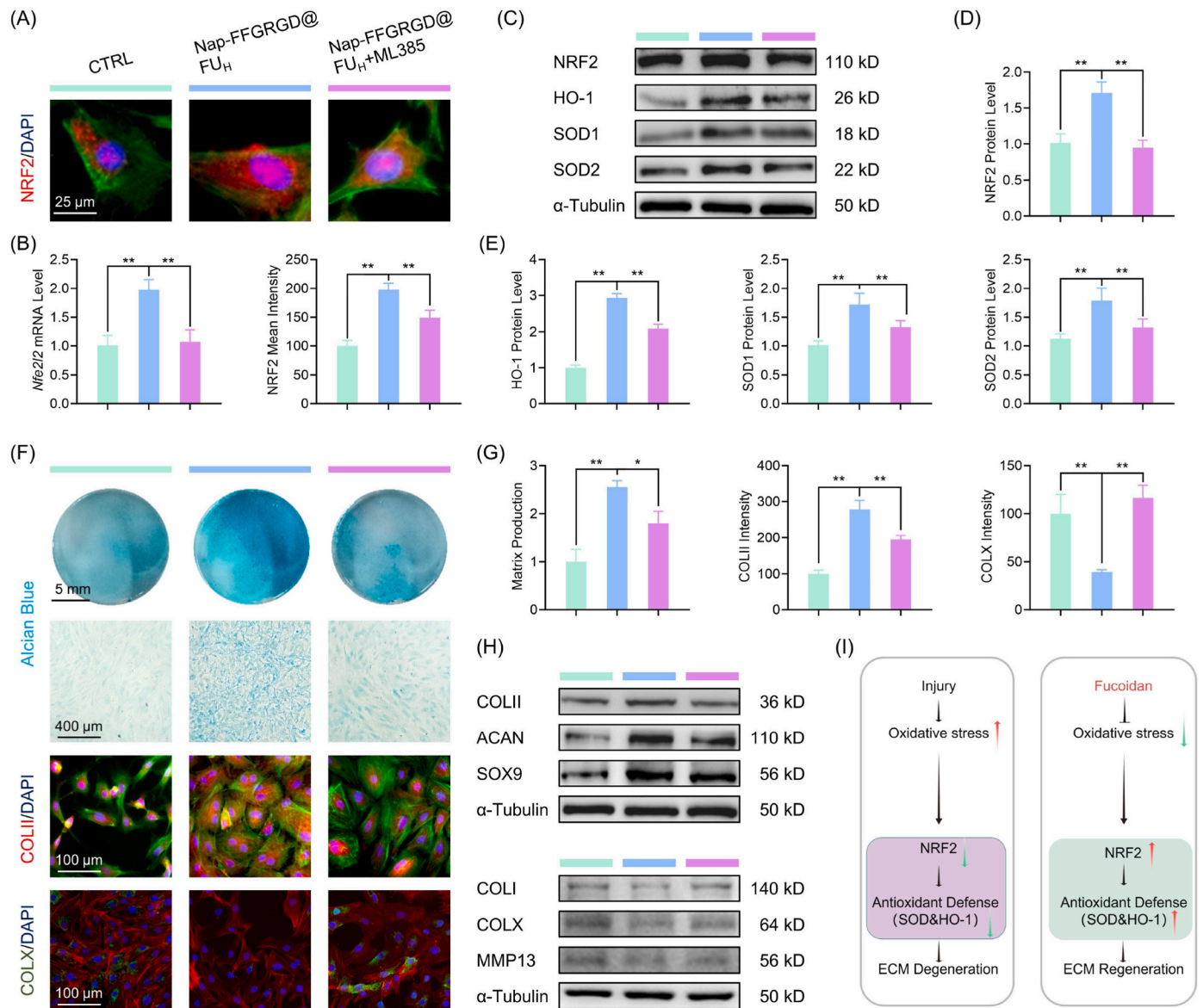


Fig. 4. Glycopeptide hydrogels yielded chondroprotective effects via activation of NRF2. (A) Representative images of chondrocytes stained by NRF2 immunofluorescence. (B) NRF2 expression were determined by RT-PCR and fluorescent intensity (n = 3). (C–E) Protein levels of antioxidant elements markers were measured using western blot (n = 3). (F) Representative images of ECM markers of chondrocytes stained by Alcian blue, COLII, and COLX immunofluorescence. (G) Quantitative assessment of matrix production level and intensity of COLII or COLX immunofluorescence (n = 3). (H) Protein levels of ECM synthesis and degradation markers were measured using western blot. (I) Scheme of the NRF2 cascade scheme implicated in fucoidan-mediated chondroprotection. Data are presented as mean ± SD (*P < 0.05 or **P < 0.01 between the indicated groups).

fucoidan-NRF2-antioxidant axis on cartilage metabolism, providing preliminary evidence that the activation of NRF2 induced by fucoidan and its subsequent intrinsic antioxidant cascade should serve as a potent enhancer for ECM remodeling (Fig. 4I). Nonetheless, the potential oscillator upon NRF2, particularly under cartilage repair conditions, remains to be clarified. Classical theory opines that the down-regulation of Kelch-like-ECH-associated protein 1 (KEAP1)-dependent ubiquitination of NRF2 acts as a primary source of newly synthesized NRF2 [46]. Our prior study demonstrated that non-coding microRNA-146a-5p (miR-146a-5p) blocks the translational process of NRF2 by targeting 3' untranslated regions (3' UTRs) to amplify inflammation-induced cartilage destruction [47]. Future research will continue to uncover the novel regulation underpinning the antioxidant effects of fucoidan.

2.5. Glycopeptide hydrogels facilitated cartilage regeneration through redox rejuvenation

A full-thickness cartilage defect was created and subsequently filled with hydrogels in a rabbit model to assess the potential therapeutic effects of glycopeptide biomimetic hydrogels on cartilage regeneration *in vivo*. The rabbits treated with Nap-FFGRGD@FU_H exhibited optimal cartilage repair 12 weeks post-surgery, as evidenced by significantly higher ICRS and MODS scores compared to the untreated group (Fig. 5A–C). According to histological staining, implantation of glycopeptide biomimetic hydrogels also increased the regenerative area by 1.65-fold (Fig. 5D). On the front of ECM rebuilding, the Nap-FFGRGD@FU_H group displays a harmonious expression of collagen, as evidenced by an increased ratio of hyaline cartilage marker COLII to

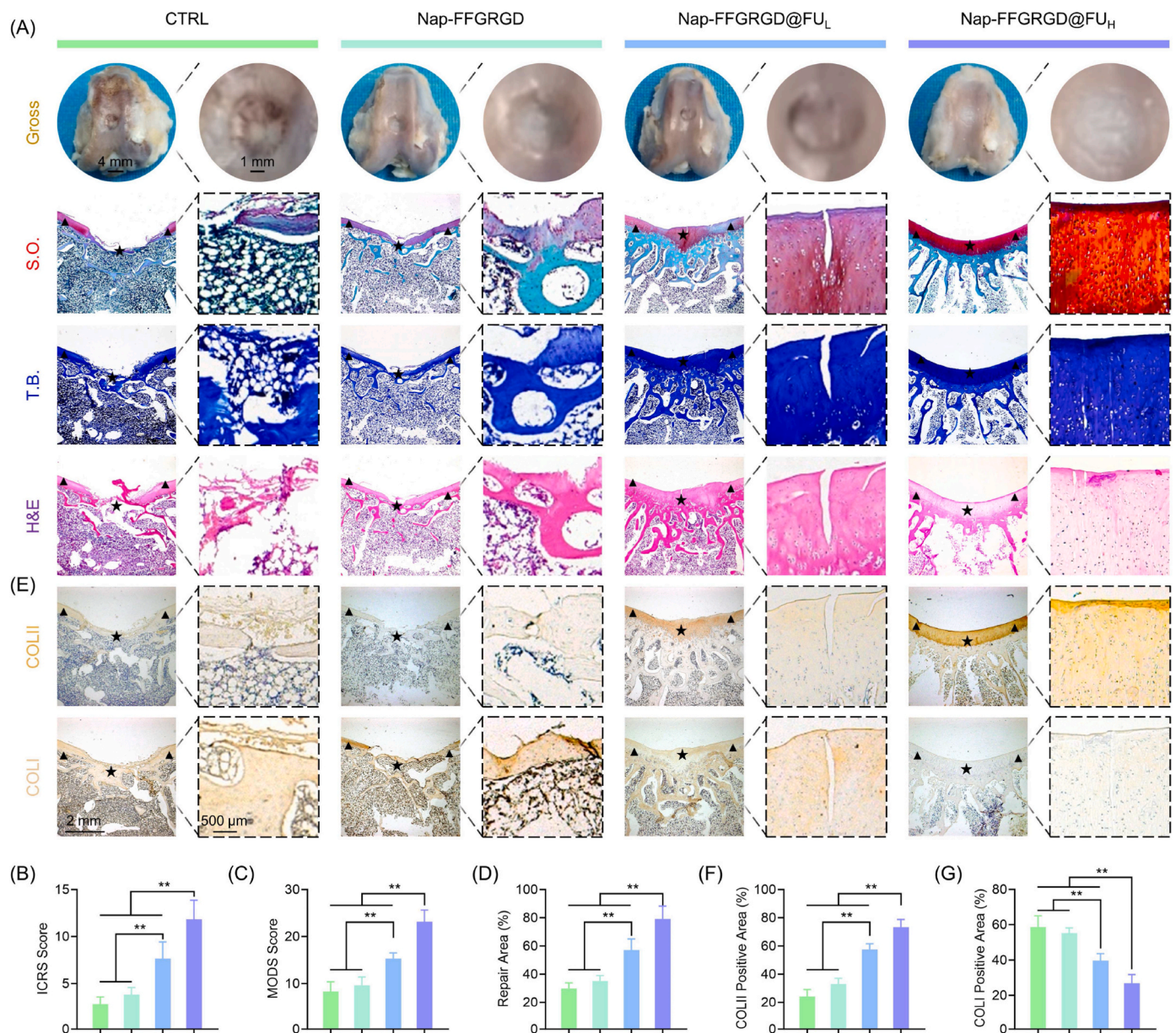


Fig. 5. Glycopeptide hydrogels boosted articular cartilage regeneration in a rabbit full-thickness cartilage defect model. (A) Representative images of gross observation of cartilage defects of the defects and histology images of trochlear groove stained by hematoxylin and eosin (H&E). Sulfated glycosaminoglycans (GAGs) were detected by Safranin O (S.O.) and toluidine blue (T.B.) staining. The triangles symbolized the encompassing indigenous cartilage, while the stars denoted the repaired tissues. (B–C) Quantification of cartilage repair using ICRS and MODS system ($n = 6$). (D) Quantification of the percentage of repaired cartilage area ($n = 6$). (E) Representative immunohistochemical (IHC) images of trochlear groove stained by COLII or COLI. (F–G) Quantification of the percentage of positively stained areas for COLII or COLI ($n = 6$). Data are presented as mean \pm SD (* $P < 0.05$ or ** $P < 0.01$ between the indicated groups).

fibrous cartilage marker COL1 (Fig. 5E–G). Moreover, treatment with glycopeptide hydrogels demonstrated a remarkable improvement in the process of subchondral bone remodeling (Fig. 6A–B&S14). Importantly, the glycopeptide hydrogels elicited endogenous NRF2 activation and its downstream pathways, as evidenced by elevated expression of SOD2 and HO-1 (Fig. 6C–F). Accordingly, the glycopeptide hydrogels significantly inhibited the level of oxidative DNA damage marker 8-OHdG, indicating a rebalanced antioxidant/pro-oxidant equilibrium for local ROS damage (Fig. 6G–H). Standard tissue engineering comprises three key elements, including cells, materials, and cytokines, which have been extensively used for CTE [48]. Nonetheless, cell viability following transplantation or immune rejection limits the generalization to clinical practice. Mimicking ECM is a novel direction for tissue-adaptive biomaterial design, allowing cell adhesion, proliferation, or

differentiation by autologous cell mobilization [49]. Owing to cartilage ECM is heterogeneous in composition, well-designed biomimetic materials that simultaneously process collagen and proteoglycan are necessary. The RGD-enriched self-assembly peptide provides an ideal environment for cell attachment, which is required to recruit neighboring stem cells for tissue reconstruction. On the other hand, fucoidan incorporation into an innovatively constructed glycopeptide structure increases biological activities and renders key polysaccharide components to an extraordinary ECM-driven agenda for cartilage repair. By mimicking natural hyaluronic acid molecules, supramolecular GAG-like glycopeptide nanofibers induce chondrogenesis and healing of osteochondral defects [50]. Importantly, the fucoidan-reinforced antioxidant properties can effectively eliminate local accumulation of ROS, thereby creating a redox-friendly microenvironment for tissue repair and

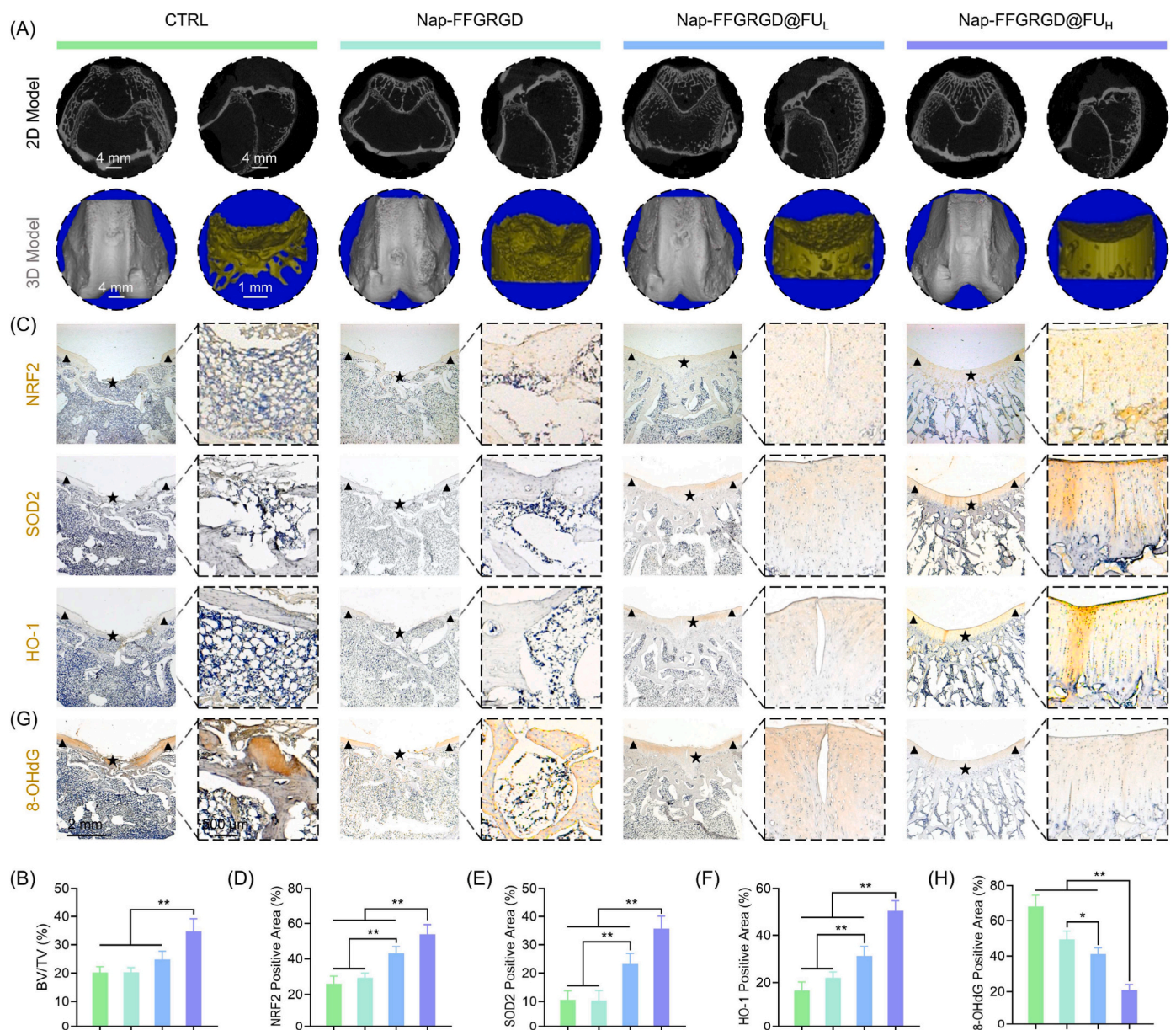


Fig. 6. Glycopeptide hydrogels facilitated cartilage regeneration through redox rejuvenation. (A) Representative images micro-CT coronal, sagittal, or 3D reconstructed view of the defects. (B) Quantification of the bone morphometric bone volume (BV) versus tissue volume (TV) value ($n = 6$). (C) Representative Immunohistochemical (IHC) images of trochlear groove stained by NRF2, SOD2, HO-1. The triangles symbolized the encompassing indigenous cartilage, while the stars denoted the repaired tissues. (D–F) Quantification of the percentage of positively stained areas for NRF2, SOD2, HO-1 ($n = 6$). (G) Representative IHC images of trochlear groove stained by 8-OHdG. (H) Quantification of the percentage of positively stained areas for 8-OHdG ($n = 6$). Data are presented as mean \pm SD (* $P < 0.05$ or ** $P < 0.01$ between the indicated groups).

regeneration.

3. Conclusion

A self-assembly glycopeptide hydrogel incorporating RGD-functional peptide and polysaccharide fucoidan was rationally developed to mimic an adaptive ECM, inspired by a natural structure of hyaline cartilage. Co-cultivation of chondrocytes with glycopeptide hydrogels not only enhanced the deposition of cartilage ECM, but also improved intracellular antioxidant properties to counteract ROS damage. Mechanistically, the chondroprotective effects of glycopeptide hydrogels were dependent upon the activation of the NRF2-associated antioxidant signaling pathways. The *in-situ* implantation of glycopeptide hydrogels facilitated the generation of novel cartilage and reinstated collagen balance by reorganizing local redox equilibrium. Overall, our proposed glycopeptide-based ECM biomimetic strategy holds immense potential for cartilage regeneration, while activation of the fucoidan-NRF2-antioxidant axis has the capacity to revolutionize bionic therapies in tissue engineering.

4. Material and methods

4.1. Preparation of glycopeptide hydrogels

Nap-FFGRGD peptide (10 mg, PeptideValley, Nanjing, China) was dissolved in 1 mL of PBS solution (pH = 7.4) to form a precursor of the hydrogel. 0.2 μ L of 1 M Na₂CO₃ solution was incrementally added, followed by thorough stirring and pH measurement using ultra-sensitive pH test paper until a pH value of 7.4 was achieved. The mixture was heated to 90 °C using a metal bath until the compound achieved transparency, followed by rapid hydrogel formation upon cooling to room temperature. To prepare the glycopeptide hydrogels with varying concentrations, 1 mg or 10 mg of fucoidan (Sigma-Aldrich, St Louis, MO, USA) were respectively dissolved in 1 mL of PBS. After being completely dissolved, 10 mg of Nap-FFGRGD polypeptide was added to the solution containing fucoidan. After thorough mixing, the solution was adjusted to a pH of 7.4. Subsequently, the self-assembled glycopeptide hydrogels were formed through a heating and cooling process. Following this, the hydrogels were utilized for animal and cell experiments.

4.2. Rheology test

Rheological properties of hydrogels were measured using a strained-controlled rheometer (AR 2000ex, TA Instruments) with a parallel plate geometry (40 mm diameter) and a gap of 500 μ m. A dynamic frequency sweep between 0.1 and 100 rad s⁻¹ was performed at a strain of 1%. Notably, all samples were measured at 37 °C.

4.3. Fourier transform infrared spectroscopy test (FTIR)

The FTIR spectra were acquired using the Thermo Nicolet 6700 FTIR instrument (Thermo Fisher Scientific, Waltham, MA, USA) equipped with attenuated total reflection (ATR) mode. The hydrogels (100 μ L) were freeze-dried and finely powdered before being deposited onto the ATR diamond crystal. After performing a background scan using the PBS buffer, each sample was subjected to 64 scans with a resolution of 4000 and 400 cm⁻¹ using the FTIR spectrometer for spectral recording.

4.4. Scanning electron microscope (SEM)

The hydrogels were fixed with 2.5% neutral glutaraldehyde for a duration of 4 h. Following PBS washing, the samples were subjected to dehydration using gradient concentrations of alcohol (50%, 60%, 70%, 80%, and 90% each for an hour, followed by complete immersion in 100% alcohol for 2 h). The samples were subsequently dehydrated using a carbon dioxide critical dryer (Tousimis, Rockville, MD, USA). The SEM images were acquired using a Zeiss Merlin scanning electron microscope

(Germany) equipped with an in-lens detector, operating at an acceleration voltage of 3 kV.

4.5. Transmission electron microscopy (TEM)

The microstructure of hydrogel samples was observed using a MODEL H-800 electron microscope at an acceleration voltage of 100 kV. A CDD camera was used to acquire digital images. All samples were applied onto carbon-coated copper grids. Subsequently, 10 μ L of uranium acetate was added to dye samples. Excess dye was removed using a clean filter paper, then the gels were overnight dried in a dryer.

4.6. Biodegradability assays

The glycopeptide hydrogel samples (1 wt%, 500 μ L) were incubated in PBS (5 mL/sample) or PBS (5 mL/sample) containing 1 ng/mL collagenase type I (Thermo Fisher Scientific) at a temperature of 37 °C and a CO₂ concentration of 5% in a humidified shaker incubator for durations of 1, 3, 5, 7, 14, and 21 days. The immersion extracts were replaced on a daily basis, and each sample was measured using an ultra-high precision electronic scale after the drying process. The initial weight is represented as W₀. The weight of the degraded hydrogel is indicated as W_n. The degradation rate (%) can be calculated using the formula: (W₀-W_n)/W₀ × 100%.

4.7. Fucoidan release

The glycopeptide hydrogel samples (500 μ L/well) were prepared in 6-well transwell chamber and incubated in 5 mL of PBS buffer. The concentrations of fucoidan were measured by aspirating 2.5 mL sample solutions at predetermined time points (1, 5, 7, and 12 h; and 1, 3, 5, 7, 14, and 21 days). An equal volume of PBS was added to the plates. The aspirate was then mixed with toluidine blue O (TBO) (Sigma-Aldrich) to form a complex prior to the addition of n-hexane. The supernatant was subjected to spectrophotometric analysis at 631 nm using a microplate spectrophotometer (Bio-Tek, Winooski, VT, USA) after 1 min of incubation. The obtained absorbance value corresponded to the concentration of fucoidan.

4.8. In vivo imaging systems (IVIS) imaging

The degradation of glycopeptide hydrogels in the joint cavity of mice was evaluated using the IVIS *in vivo* imaging system (Spectrum, PerkinElmer). After mice were anesthetized with isopentane, 10 μ L of Cy5-labeled glycopeptide hydrogel (10 mg/mL) was injected into the joint cavity of each mouse. Days 1, 7, 14, and 21 later, the mice were anesthetized using the same method. The mice were meticulously positioned on the imaging chamber stage upon completion and testing temperature was maintained at 37 °C, and the exposure procedure was conducted. The exposure duration and imaging parameters were adjusted to optimize visualization and parameters were consistently maintained for each subsequent imaging session. Imaging kinetic curves were acquired after completing the imaging of all mice. The region of interest (ROI) was defined as the joint cavity area in each mouse. The IVIS imaging system (Xenogen) was utilized for the integration of bioluminescence signals. The imaging signals were quantified to determine the average radiance, and the resulting ROI photon flux was considered indicative of hydrogel retention in the joint cavity of mice.

4.9. Mechanical test

The hydrogels were prepared into cylindrical shapes (diameter: 1 cm, height: 4 mm) through a heating-cooling process in order to evaluate their compressive mechanical properties. The hydrogels were incubated at 4 °C overnight to facilitate the formation of a stable self-assembling peptide system. Subsequently, each of the three samples

was meticulously transferred onto the testing platform. The excess water around the sample is blotted with filter paper. The hydrogels were subjected to uniaxial compression experimental testing using a mechanical testing system, with a test speed of 1 mm/min, until failure occurred.

4.10. Isolation and culture for rabbit articular chondrocytes

After administering anesthesia, articular cartilage tissue was harvested from 6-week-old New Zealand white rabbits. Two rabbits were utilized simultaneously to procure chondrocytes from the condyles of femur for subsequent experimental procedures. Thereafter, samples were sectioned into small fragments and digested within 0.4 % collagenase II (Gibco, USA) in a humidified 37 °C, 5 % CO₂ incubator. Primary chondrocytes were filtered using a 100 µm nylon mesh (BD, Biosciences, San Jose, CA, USA). Cells were seeded into culture flasks (CoStar, Tewksbury, MA, USA) and kept in Dulbecco's modified Eagle's medium/nutrient mixture F-12 (DMEM/F12) with 10 % fetal bovine serum (FBS, Gibco, heat-inactivated), penicillin (100 U/mL final concentration) and streptomycin (100 U/mL). Chondrocytes at passage one were used for subsequent experiments.

4.11. Co-culture of glycopeptide hydrogels and chondrocytes

The transwell chamber was selected as the optimal platform for the co-culture of hydrogels and chondrocytes. Initially, the hydrogel was seeded in the upper chamber while chondrocytes were seeded in the lower chamber. The upper chamber was fully immersed in DMEM/F12 medium to ensure complete coverage of the hydrogel. The RT-PCR, western blotting, fucoidan release, and hydrogel degradation experiments were conducted in six-well plates, with a hydrogel volume of 500 µL in the upper chamber and a culture medium volume of 5 mL. The cytological and immunofluorescent stains were performed in 24-well plates, with a hydrogel volume of 125 µL in the upper chamber and a culture medium volume of 1.25 mL. The cell proliferation assays were conducted using 96-well plates, with a hydrogel volume of 31.25 µL in the upper chamber and a culture medium volume of 312.5 µL. The medium in the above co-culture system was replaced at 12 h, day one, day two, and day five respectively.

4.12. Cell proliferation test

Cell proliferation was measured using the Cell Counting Kit-8 (CCK-8, Beyotime, Shanghai, China). Briefly, 3000 cells were seeded into 96-well plates. After 24 h, cells were co-cultured with different hydrogel samples for 1, 3, 5, and 7 days as mentioned above. Subsequently, the CCK-8 solution was added to 96-well plates for 2 h at 37 °C. The absorbance was measured at 450 nm using a microplate spectrophotometer (Bio-Tek).

4.13. Cytoskeleton staining

Staining was performed using the phalloidin kit (Abcam, Waltham, MA, USA) as per the manufacturer's instructions. After being incubated with hydrogels for a duration of seven days, the cells were fixed using 4 % paraformaldehyde (PFA) for 30 min. Cells were incubated with FITC-phalloidin dilution (1:500) for 30 min in the dark to stain the F-actin. Nuclei were counterstained with DAPI (Invitrogen, Carlsbad, CA, USA) for 1 min. Images were observed under a microscope (Zeiss, AxioImager, Germany).

4.14. Live/dead staining

Cell toxicity of the hydrogels was performed using a Live/dead cell staining kit (Beyotime). Briefly, cells were cultured in the 24-well plates (10⁵ cells/well) and incubated with hydrogels for seven days. Afterward,

cells were incubated at 37 °C for 30 min with fluorescent buffer as per the manufacturer's recommendations. After washing twice with PBS, live (green) or dead (red) chondrocytes were observed under a fluorescence microscope (Zeiss AxioImager, Germany). The semi-quantitative analysis of live/dead cell staining images was determined utilizing the Image J software.

4.15. Immunofluorescence staining

After being incubated with hydrogels for a duration of seven days, cells were fixed with 4 % PFA for 30 min. After washing twice with PBS and permeabilization with 0.3 % Triton (Sigma-Aldrich), cells were blocked using bovine serum albumin (BSA) at room temperature for 1 h. Subsequently, cells were incubated with primary antibody (COLII, ab34712 or NRF2, ab62352) with appropriate dilutions (1:500) overnight at 4 °C. Cells were then washed three times with PBS, before staining with the corresponding secondary antibody (ab150075, 1:500) for 1 h. Nuclei were counterstained with DAPI for 1 min. Images were captured using a Zeiss Axiovert 40CFL fluorescence microscope. The fluorescence intensity analysis was conducted using the Image J software. Briefly, the fluorescence images were adjusted to 16-bit single-channel mode through the software, while also removing background color and optimizing parameters such as threshold to maximize inclusion of valid fluorescence signals. The region of interest (ROI) was selected to fluorescence intensity of all pixels within the designated area, the average fluorescence intensity within the ROI was calculated.

4.16. Alcian blue staining

The hydrogels and cells were co-cultured following the aforementioned protocol. After the seven days, the medium was discarded and rinsed with PBS buffer. The samples were then fixed with 4 % paraformaldehyde at room temperature for 30 min. After washing, a solution of Alcian blue staining (Sigma-Aldrich) was added to each well of a 24-well plate (200 µL/well), and the plate was stained at room temperature for 1 h. The images were observed and collected using an Olympus IX73 inverted microscope, followed by rinsing with deionized water. The Alcian blue level, representing the deposition of glycosaminoglycan chondrocyte matrix, was analyzed using Image J software. The RGB channels of the images were converted to mode with a 16-bit depth. Subsequently, the parameters were adjusted and an appropriate ROI was selected gray value analysis after eliminating the background color. The average Alcian blue percentage was calculated by dividing the gray value by the area of ROI. The Alcian blue percentage of the control group was standardized to 100 % for statistical analysis.

4.17. Intracellular and mitochondrial ROS levels

Chondrocytes were seeded at a density of 20,000 cells per well in 24-well cell culture plates and co-cultured with hydrogel using the aforementioned method. When the cell confluence reaches 60–70 % on day 7, remove the medium and carefully wash with PBS. DCFH-DA (Beyotime Biotechnology) or MitoSOX (Thermo Fisher Scientific, USA) staining working solution (prepared by mixing DCFH-DA or MitoSOX in a ratio of 1:1000 with DMEM/F12 medium) was added to the 24-well plate and incubated at 37 °C in a dark cell culture incubator for 30 min. The nucleus was subsequently counterstained with a nuclear dye for a duration of 1 min. The images were subsequently acquired using a fluorescence microscope and the average fluorescence intensity within the ROI was calculated using the Image J software.

4.18. Real-time polymerase chain reaction (RT-PCR)

The hydrogels and cells were co-cultured following the aforementioned protocol. After the seven days, total RNA was isolated by Trizol reagent (Invitrogen) and the concentration of samples was calculated

using NanoDrop2000 (Thermo Fisher Scientific, USA). RNA was reversely transcribed into cDNA using reverse transcription reagents (TaKaRa, Shiga, Japan). RT-PCR was performed on a CFX96 Real-Time system (Bio-Rad, Shanghai, China). Gene expression levels were normalized with glyceraldehyde 3-phosphate dehydrogenase (*Gapdh*) expression as endogenous control and then analyzed using the Ct ($2^{-\Delta\Delta Ct}$) method. Primer sequences are available in [Supplementary Table 1](#).

4.19. Western blot analysis

Total protein was isolated from chondrocytes using RIPA buffer (Beyotime). Protein concentration was measured using the BCA protein assay kit (Beyotime). An equivalent protein of each sample was separated using 10 % SDS-PAGE, then transferred to nitrocellulose membranes. The membranes were blocked using Western blocking buffer (Beyotime) at room temperature for 1 h then incubated overnight with the following primary antibodies at 4 °C: COLII (ab188570, 1:5000), ACAN (ab3778, 1:3000), SOX9 (A19710, 1:3000), MMP13 (A11148, 1:2000), COLI (A16891, 1:2000), COLX (ab58632, 1:2000), NRF2 (ab62352, 1:5000), HO-1 (ab52947, 1:5000), SOD1 (ab52950, 1:5000), SOD2 (ab68155, 1:5000), ND4 (A9941, 1:2000), SDHA (A13852, 1:2000), COX4I2 (A6564, 1:2000), ATP5A (A11217, 1:2000), or α -Tubulin (ab7291, 1:5000). After washing twice with TBST, the blots were incubated with corresponding HRP-conjugated secondary antibodies (Abcam) at room temperature for 1 h. The protein bonds were observed with a chemiluminescence detection system (Bio-Rad).

4.20. RNA sequencing and bioinformatic analysis

The Gene Expression Omnibus datasets were utilized for and downloading the identified GSE169077, which comprised 5 normal samples and 6 osteoarthritis cartilage samples, based on the Genome-wide U133A Affymetrix oligonucleotide array. The genes that exhibited a false discovery rate (FDR) of less than 0.05 and a fold change greater than 2 were considered as differentially expressed genes (DEGs). Enrichment analysis was conducted utilizing gene ontology (GO) and Kyoto Encyclopedia of Genes and Genomes (KEGG) pathways analysis.

4.21. Rabbit models with a full-thickness cartilage defect

The protocol was approved by the Ethics Committee of Soochow University (Ethics approval number: SUDA20221009A02). New Zealand white rabbits (2.2–2.4 kg) were to build cartilage defects model for evaluating the regenerate effect of various hydrogel samples. A dose of 30 mg/kg of 3 % sodium pentobarbital was administered via the rabbit ear margin vein. After the rabbits were anesthetized, the knee joint was incised and the surrounding tissues were carefully isolated. Thereafter, the femoral trochlea was exposed, then an electric drill was used to create a hole (height: 3 mm, diameter: 4 mm). The defect regions were implanted with 40 μ L of glycopeptide hydrogel according to grouping, while the blank control group underwent drilling without hydrogel implantation. Each experimental group consisted of three rabbits with a bilateral defect model. The rabbits received a three-day course of post-operative penicillin (100,000 U/kg) to combat infection, while daily monitoring the progress of incision healing. After a duration of 12 weeks, the animals were humanely euthanized, following which the femoral condyles were harvested for subsequent experimental procedures.

4.22. Micro-CT analysis

The New Zealand white rabbits used as a model for cartilage defects were humanely euthanized, and distal femoral specimens were obtained 12 weeks post-surgery. The muscles and ligaments surrounding the joint were meticulously dissected. Subsequently, fixed in a 4 %

paraformaldehyde solution for 48 h, and the femoral trochlea samples underwent analysis using a high-resolution Micro-CT system (SkyScan 1176, Aartselaar, Belgium). The initial scan was conducted at 60 kV, 170 mA, and 0.7° with an 18 μ m resolution. The specimen was positioned on the testing station and scanned using consistent parameters. Each specimen underwent a 20-min testing process to ensure the integrity of the scanned layers, followed by reconstruction and qualitative analysis of three-dimensional microstructure images using NRecon and Data Viewer software. The defect site was defined as a ROI for the assessment of bone volume to tissue volume ratio (BV/TV), trabecular separation (T.Sp), trabecular thickness (Tb.Th), and trabecular number (Tb.N). These parameters were utilized to evaluate both bone density and microstructure.

4.23. Histological staining and immunohistochemistry

Samples of femoral trochlea were fixed in 4 % paraformaldehyde at room temperature for 48 h. The samples were decalcified with 10 % EDTA (pH = 7.4, Sigma-Aldrich) and embedded in paraffin (Leica, Germany). Tissues were sectioned into slices of 6 μ m thickness. To examine cartilage deposition, the specimens were stained using hematoxylin and eosin (H&E, Sigma-Aldrich), Safranin O/Fast Green (S.O., Sigma-Aldrich), and Toluidine Blue O (T.B., Beyotime) following the manufacturer's instructions. The specimens of tissue were imaged under an optical microscope. Cartilage regeneration was evaluated using the International Cartilage Repair Society system (ICRS) [51] or modified O'Driscoll scale (MODS) [52]. The regenerative area percentage was determined by calculating the proportion of the defect surface covered with repaired tissue, using the formula: (original defect area - defect area at sacrifice)/original defect area \times 100 % [53]. Tissue slices were heated and dewaxed in xylene for IHC staining. Afterward, they were dehydrated in gradient ethanol before antigen retrieval and blocking using goat serum. Slices were overnight incubated with primary antibodies against COLII, COLI, or NRF2 at 4 °C. Secondary antibody (Vector Laboratories, Burlingame, CA, USA) was selected to incubate sections at room temperature for 1 h, followed by treatment with ABC kit (Vector) and color development with DAB Substrate (Vector). Slides were observed and imaged under an optical microscope. The Image J software was used to analyze the percentage of positive cells. The detailed information regarding histological assessment criteria was provided in [Supplementary Tables 2 and 3](#)

4.24. Statistical analysis

All values were presented as the standard error (mean \pm SD). All statistical analyses were performed using the GraphPad Prism 9.3 software. For normally distributed data, Student's t-test and One-Way ANOVA were used for two groups and multiple groups, respectively; the Mann-Whitney *U* test or Kruskal-Wallis test were used to analyze for non-normal distribution. *P* value < 0.05 was considered statistically significant.

Consent for publication

All authors are consent for publication.

Availability of data and materials

The data that support the findings of this study are available from the corresponding author upon reasonable request.

Funding

This work was supported by grants from National Key R&D Program of China (Grant Nos: 2022YFC2502902), National Natural Science Foundation of China (Grant Nos: 82072442, 82272494, 82072082 and

32122046), the Priority Academic Program Development of Jiangsu Higher Education Institutions (PAPD), and the Shenzhen Fundamental Research Foundation (Grant Nos. JCYJ20210324115814040 and JCYJ20210324113001005).

Ethics approval and consent to participate

All animal experiments were approved by the Ethics Committee of Soochow University.

CRediT authorship contribution statement

Zhijian Zhao: Data curation, Formal analysis, Methodology. **Xiao-wei Xia:** Data curation, Resources, Software. **Junlin Liu:** Formal analysis, Software. **Mingzhuang Hou:** Data curation, Validation. **Yang Liu:** Investigation, Methodology. **Zhangzhe Zhou:** Data curation, Methodology. **Yong Xu:** Supervision, Validation. **Fan He:** Formal analysis, Resources. **Huilin Yang:** Supervision, Validation. **Yijian Zhang:** Conceptualization, Writing – original draft. **Changshun Ruan:** Supervision, Writing – review & editing. **Xuesong Zhu:** Funding acquisition, Project administration.

Declaration of competing interest

The authors declare that the research was conducted in the absence of any commercial or financial relationships that could be construed as a potential conflict of interest.

Appendix A. Supplementary data

Supplementary data to this article can be found online at <https://doi.org/10.1016/j.bioactmat.2023.10.013>.

References

- [1] S. Macmull, J.A. Skinner, G. Bentley, R.W. Carrington, T.W. Briggs, Treating articular cartilage injuries of the knee in young people, *BMJ* 340 (2010) e998.
- [2] K. Mithoefer, L. Peterson, M. Zenobi-Wong, B.R. Mandelbaum, Cartilage issues in football-today's problems and tomorrow's solutions, *Br. J. Sports Med.* 49 (9) (2015) 590–596.
- [3] W. Li, J. Lai, Y. Zu, P. Lai, Cartilage-inspired hydrogel lubrication strategy, *Innovation* 3 (5) (2022), 100275.
- [4] C. Li, Y. Du, T. Zhang, H. Wang, Z. Hou, Y. Zhang, W. Cui, W. Chen, "Genetic scissors" CRISPR/Cas9 genome editing cutting-edge biocarrier technology for bone and cartilage repair, *Bioact. Mater.* 22 (2023) 254–273.
- [5] Y. Hu, H. Zhang, S. Wang, L. Cao, F. Zhou, Y. Jing, J. Su, Bone/cartilage organoid on-chip: construction strategy and application, *Bioact. Mater.* 25 (2023) 29–41.
- [6] B.J. Klotz, D. Gawlipta, A. Rosenberg, J. Malda, F.P.W. Melchels, Gelatin-methacryloyl hydrogels: towards biofabrication-based tissue repair, *Trends Biotechnol.* 34 (5) (2016) 394–407.
- [7] Y. Kang, H. Zhang, L. Chen, J. Dong, B. Yao, X. Yuan, D. Qin, A.V. Yaremenko, C. Liu, C. Feng, X. Ji, W. Tao, The marriage of Xenics and hydrogels: fundamentals, applications, and outlook, *Innovation* 3 (6) (2022), 100327.
- [8] J.H. Collier, J.S. Rudra, J.Z. Gasiorowski, J.P. Jung, Multi-component extracellular matrices based on peptide self-assembly, *Chem. Soc. Rev.* 39 (9) (2010) 3413–3424.
- [9] Z. Zhang, S. Ai, Z. Yang, X. Li, Peptide-based supramolecular hydrogels for local drug delivery, *Adv. Drug Deliv. Rev.* 174 (2021) 482–503.
- [10] S. Xue, X. Zhou, W. Sang, C. Wang, H. Lu, Y. Xu, Y. Zhong, L. Zhu, C. He, J. Ma, Cartilage-targeting peptide-modified dual-drug delivery nanoplatfrom with NIR laser response for osteoarthritis therapy, *Bioact. Mater.* 6 (8) (2021) 2372–2389.
- [11] K. Lu, Q. Wang, L. Hao, G. Wei, T. Wang, W.W. Lu, G. Xiao, L. Tong, X. Zhao, D. Chen, miR-204 ameliorates osteoarthritis pain by inhibiting SP1-LRP1 signaling and blocking neuro-cartilage interaction, *Bioact. Mater.* 26 (2023) 425–436.
- [12] Q. Li, Z. Gao, Y. Chen, M.X. Guan, The role of mitochondria in osteogenic, adipogenic and chondrogenic differentiation of mesenchymal stem cells, *Protein Cell* 8 (6) (2017) 439–445.
- [13] F. Han, Z. Tu, Z. Zhu, D. Liu, Q. Meng, Q. Yu, Y. Wang, J. Chen, T. Liu, F. Han, B. Li, Targeting endogenous reactive oxygen species removal and regulating regenerative microenvironment at annulus fibrosus defects promote tissue repair, *ACS Nano* 17 (8) (2023) 7645–7661.
- [14] C. Shu, C. Qin, L. Chen, Y. Wang, Z. Shi, J. Yu, J. Huang, C. Zhao, Z. Huan, C. Wu, M. Zhu, Y. Zhu, Metal-organic framework functionalized bioceramic scaffolds with antioxidant activity for enhanced osteochondral regeneration, *Adv. Sci.* 10 (13) (2023), e2206875.
- [15] K. Murakami, H. Aoki, S. Nakamura, S. Nakamura, M. Takikawa, M. Hanzawa, S. Kishimoto, H. Hattori, Y. Tanaka, T. Kiyosawa, Y. Sato, M. Ishihara, Hydrogel blends of chitin/chitosan, fucoidan and alginate as healing-impaired wound dressings, *Biomaterials* 31 (1) (2010) 83–90.
- [16] W. Zheng, Y. Hao, D. Wang, H. Huang, F. Guo, Z. Sun, P. Shen, K. Sui, C. Yuan, Q. Zhou, Preparation of triamcinolone acetonide-loaded chitosan/fucoidan hydrogel and its potential application as an oral mucosa patch, *Carbohydr. Polym.* 272 (2021), 118493.
- [17] P.A.R. Fernandes, M.A. Coimbra, The antioxidant activity of polysaccharides: a structure-function relationship overview, *Carbohydr. Polym.* 314 (2023), 120965.
- [18] J.Y. Reginster, R. Deroisy, L.C. Rovati, R.L. Lee, E. Lejeune, O. Bruyere, G. Giacovelli, Y. Henrotin, J.E. Dacre, C. Gossett, Long-term effects of glucosamine sulphate on osteoarthritis progression: a randomised, placebo-controlled clinical trial, *Lancet* 357 (9252) (2001) 251–256.
- [19] L.M. Wildi, J.P. Raynaud, J. Martel-Pelletier, A. Beaulieu, L. Bessette, F. Morin, F. Abram, M. Dorais, J.P. Pelletier, Chondroitin sulphate reduces both cartilage volume loss and bone marrow lesions in knee osteoarthritis patients starting as early as 6 months after initiation of therapy: a randomised, double-blind, placebo-controlled pilot study using MRI, *Ann. Rheum. Dis.* 70 (6) (2011) 982–989.
- [20] Y. Yao, A.M. Zaw, D.E.J. Anderson, Y. Jeong, J. Kunihiro, M.T. Hinds, E.K.F. Yim, Fucoidan and topography modification improved in situ endothelialization on acellular synthetic vascular grafts, *Bioact. Mater.* 22 (2023) 535–550.
- [21] P. Karunanithi, M.R. Murali, S. Samuel, H.R.B. Raghavendran, A.A. Abbas, T. Kamarul, Three dimensional alginate-fucoidan composite hydrogel augments the chondrogenic differentiation of mesenchymal stromal cells, *Carbohydr. Polym.* 147 (2016) 294–303.
- [22] W. Zheng, Z. Wang, L. Song, Q. Zhao, J. Zhang, D. Li, S. Wang, J. Han, X.L. Zheng, Z. Yang, D. Kong, Endothelialization and patency of RGD-functionalized vascular grafts in a rabbit carotid artery model, *Biomaterials* 33 (10) (2012) 2880–2891.
- [23] R. Pugliese, F. Gelain, Cross-linked self-assembling peptides and their post-assembly functionalization via one-pot and in situ gelation system, *Int. J. Mol. Sci.* 21 (12) (2020).
- [24] J. Zhu, S. Yang, Y. Qi, Z. Gong, H. Zhang, K. Liang, P. Shen, Y.Y. Huang, Z. Zhang, W. Ye, L. Yue, S. Fan, S. Shen, A.G. Mikos, X. Wang, X. Fang, Stem cell-homing hydrogel-based miR-29b-5p delivery promotes cartilage regeneration by suppressing senescence in an osteoarthritis rat model, *Sci. Adv.* 8 (13) (2022), eabk0011.
- [25] S. Machado, N. González-Ballesteros, A. Gonçalves, L. Magalhães, M. Sárria Pereira de Passos, M.C. Rodríguez-Argüelles, A. Castro Gomes, Toxicity in vitro and in zebrafish embryonic development of gold nanoparticles biosynthesized using cystoseira macroalgae extracts, *Int. J. Nanomed.* 16 (2021) 5017–5036.
- [26] P.K. Smith, A.K. Mallia, G.T. Hermanson, Colorimetric method for the assay of heparin content in immobilized heparin preparations, *Anal. Biochem.* 109 (2) (1980) 466–473.
- [27] B.S. Kim, H.J. Kang, J.Y. Park, J. Lee, Fucoidan promotes osteoblast differentiation via JNK- and ERK-dependent BMP2-Smad 1/5/8 signaling in human mesenchymal stem cells, *Exp. Mol. Med.* 47 (1) (2015) e128.
- [28] J.H. Lee, S.H. Lee, S.H. Choi, T. Asahara, S.M. Kwon, The sulfated polysaccharide fucoidan rescues senescence of endothelial colony-forming cells for ischemic repair, *Stem Cell.* 33 (6) (2015) 1939–1951.
- [29] C. Vaamonde-García, N. Flórez-Fernández, M.D. Torres, M.J. Lamas-Vázquez, F. J. Blanco, H. Domínguez, R. Meijide-Failde, Study of fucoidans as natural biomolecules for therapeutic applications in osteoarthritis, *Carbohydr. Polym.* 258 (2021), 117692.
- [30] Y. Lei, Y. Wang, J. Shen, Z. Cai, Y. Zeng, P. Zhao, J. Liao, C. Lian, N. Hu, X. Luo, W. Cui, W. Huang, Stem cell-recruiting injectable microgels for repairing osteoarthritis, *Adv. Funct. Mater.* 31 (48) (2021), 2105084.
- [31] J.H. Fitton, Therapies from fucoidan; multifunctional marine polymers, *Mar. Drugs* 9 (10) (2011) 1731–1760.
- [32] M. Piñeiro-Ramil, N. Flórez-Fernández, O. Ramil-Gómez, M.D. Torres, H. Domínguez, F.J. Blanco, R. Meijide-Failde, C. Vaamonde-García, Antifibrotic effect of brown algae-derived fucoidans on osteoarthritic fibroblast-like synoviocytes, *Carbohydr. Polym.* 282 (2022), 119134.
- [33] S.B. Park, K.R. Chun, J.K. Kim, K. Suk, Y.M. Jung, W.H. Lee, The differential effect of high and low molecular weight fucoidans on the severity of collagen-induced arthritis in mice, *Phytother. Res.* 24 (9) (2010) 1384–1391.
- [34] A. De Pieri, S. Rana, S. Korntner, D.I. Zeugolis, Seaweed polysaccharides as macromolecular crowding agents, *Int. J. Biol. Macromol.* 164 (2020) 434–446.
- [35] H.T. Lu, W.T. Chang, M.L. Tsai, C.H. Chen, W.Y. Chen, F.L. Mi, Development of injectable fucoidan and biological macromolecules hybrid hydrogels for intra-articular delivery of platelet-rich plasma, *Mar. Drugs* 17 (4) (2019) 236.
- [36] H. Raghun, C.M. Lepus, Q. Wang, H.H. Wong, N. Lingampalli, F. Oliviero, L. Punzi, N.J. Giori, S.B. Goodman, C.R. Chu, J.B. Sokolove, W.H. Robinson, CCL2/CCR2, but not CCL5/CCR5, mediates monocyte recruitment, inflammation and cartilage destruction in osteoarthritis, *Ann. Rheum. Dis.* 76 (5) (2017) 914–922.
- [37] Q. Yu, F. Han, Z. Yuan, Z. Zhu, C. Liu, Z. Tu, Q. Guo, R. Zhao, W. Zhang, H. Wang, H. Mao, B. Li, C. Zhu, Fucoidan-loaded nanofibrous scaffolds promote annulus fibrosus repair by ameliorating the inflammatory and oxidative microenvironment in degenerative intervertebral discs, *Acta Biomater.* 148 (2022) 73–89.
- [38] F.J. Blanco, I. Rego, C. Ruiz-Romero, The role of mitochondria in osteoarthritis, *Nat. Rev. Rheumatol.* 7 (3) (2011) 161–169.
- [39] Y. Zhang, M. Hou, Y. Liu, T. Liu, X. Chen, Q. Shi, D. Geng, H. Yang, F. He, X. Zhu, Recharge of chondrocyte mitochondria by sustained release of melatonin protects cartilage matrix homeostasis in osteoarthritis, *J. Pineal Res.* 73 (2) (2022), e12815.
- [40] Y. Zhang, Y. Liu, M. Hou, X. Xia, J. Liu, Y. Xu, Q. Shi, Z. Zhang, L. Wang, Y. Shen, H. Yang, F. He, X. Zhu, Reprogramming of mitochondrial respiratory chain

- complex by targeting SIRT3-COX4I2 Axis attenuates osteoarthritis progression, *Adv. Sci.* 10 (10) (2023), e2206144.
- [41] I.P.S. Fernando, K.K.A. Sanjeeva, H.G. Lee, H.S. Kim, A. Vaas, H.I.C. De Silva, C. M. Nanayakkara, D.T.U. Abeytungga, D.S. Lee, J.S. Lee, Y.J. Jeon, Fucoidan purified from *Sargassum polycystum* induces apoptosis through mitochondria-mediated pathway in HL-60 and MCF-7 cells, *Mar. Drugs* 18 (4) (2020) 196.
- [42] C.J. Wruck, A. Fragoulis, A. Gurzynski, L.O. Brandenburg, Y.W. Kan, K. Chan, J. Hassenpflug, S. Freitag-Wolf, D. Varoga, S. Lippross, T. Pufe, Role of oxidative stress in rheumatoid arthritis: insights from the Nrf2-knockout mice, *Ann. Rheum. Dis.* 70 (5) (2011) 844–850.
- [43] D. Cai, S. Yin, J. Yang, Q. Jiang, W. Cao, Histone deacetylase inhibition activates Nrf2 and protects against osteoarthritis, *Arthritis Res. Ther.* 17 (2015) 269.
- [44] M. Hou, Y. Zhang, X. Zhou, T. Liu, H. Yang, X. Chen, F. He, X. Zhu, Kartogenin prevents cartilage degradation and alleviates osteoarthritis progression in mice via the miR-146a/NRF2 axis, *Cell Death Dis.* 12 (5) (2021) 483.
- [45] M.S. Zahan, A. Hasan, M.H. Rahman, K.N. Meem, A. Moni, M.A. Hannan, M. J. Uddin, Protective effects of fucoidan against kidney diseases: pharmacological insights and future perspectives, *Int. J. Biol. Macromol.* 209 (Pt B) (2022) 2119–2129.
- [46] S. Adinolfi, T. Patinen, A. Jawahar Deen, S. Pitkänen, J. Härkönen, E. Kansanen, J. Küblbeck, A.L. Levonen, The KEAP1-NRF2 pathway: targets for therapy and role in cancer, *Redox Biol.* 63 (2023), 102726.
- [47] X. Zhou, Y. Zhang, M. Hou, H. Liu, H. Yang, X. Chen, T. Liu, F. He, X. Zhu, Melatonin prevents cartilage degradation in early-stage osteoarthritis through activation of miR-146a/NRF2/HO-1 Axis, *J. Bone Miner. Res.* 37 (5) (2022) 1056–1072.
- [48] W. Wei, Y. Ma, X. Yao, W. Zhou, X. Wang, C. Li, J. Lin, Q. He, S. Leptihn, H. Ouyang, Advanced hydrogels for the repair of cartilage defects and regeneration, *Bioact. Mater.* 6 (4) (2021) 998–1011.
- [49] J.M. Coburn, M. Gibson, S. Monagle, Z. Patterson, J.H. Elisseeff, Bioinspired nanofibers support chondrogenesis for articular cartilage repair, *Proc. Natl. Acad. Sci. U.S.A.* 109 (25) (2012) 10012–10017.
- [50] S. Ustun Yaylaci, M. Sardan Ekiz, E. Arslan, N. Can, E. Kilic, H. Ozkan, I. Orujalipoor, S. Ide, A.B. Tekinay, M.O. Guler, Supramolecular GAG-like self-assembled glycopeptide nanofibers induce chondrogenesis and cartilage regeneration, *Biomacromolecules* 17 (2) (2016) 679–689.
- [51] P. Mainil-Varlet, T. Aigner, M. Brittberg, P. Bullough, A. Hollander, E. Hunziker, R. Kandel, S. Nehrer, K. Pritzker, S. Roberts, E. Stauffer, Histological assessment of cartilage repair: a report by the histology endpoint committee of the international cartilage repair society (ICRS), *J. Bone Joint Surg. Am.* 85-A (Suppl 2) (2003) 45–57.
- [52] S.R. Frenkel, G. Bradica, J.H. Brekke, S.M. Goldman, K. Ieska, P. Issack, M.R. Bong, H. Tian, J. Gokhale, R.D. Coutts, R.T. Kronengold, Regeneration of articular cartilage—evaluation of osteochondral defect repair in the rabbit using multiphasic implants, *Osteoarthritis Cartilage* 13 (9) (2005) 798–807.
- [53] X. Zhang, S. Wu, T. Naccarato, M. Prakash-Damani, Y. Chou, C.Q. Chu, Y. Zhu, Regeneration of hyaline-like cartilage in situ with SOX9 stimulation of bone marrow-derived mesenchymal stem cells, *PLoS One* 12 (6) (2017), e0180138.